PAPER

Atomic and electronic structures evolution of the narrow band gap semiconductor Ag_2Se under high pressure

IOP Publishing Journal of Physics: Condensed Matter
J. Phys.: Condens. Matter **28** (2016) 385801 (6pp) doi:10.1088/0953-8984/28/38/385801

Atomic and electronic structures evolution of the narrow band gap semiconductor Ag_2Se under high pressure

P Naumov[1], O Barkalov[1,2], H Mirhosseini[1], C Felser[1] and S A Medvedev[1]

[1] Max-Planck-Institute for Chemical Physics of Solids, D-01187 Dresden, Germany
[2] Institute of Solid State Physics, Russian Academy of Sciences, Academician Ossipyan str. 2, Chernogolovka, Moscow District, 142432, Russia

E-mail: medvedie@cpfs.mpg.de

Received 25 April 2016, revised 10 June 2016
Accepted for publication 28 June 2016
Published 20 July 2016

Abstract

Non-trivial electronic properties of silver telluride and other chalcogenides, such as the presence of a topological insulator state, electronic topological transitions, metallization, and the possible emergence of superconductivity under pressure have attracted attention in recent years. In this work, we studied the electronic properties of silver selenide (Ag_2Se). We performed direct current electrical resistivity measurements, *in situ* Raman spectroscopy, and synchrotron x-ray diffraction accompanied by *ab initio* calculations to explore pressure-induced changes to the atomic and electronic structure of Ag_2Se. The temperature dependence of the electrical resistivity was measured up to 30 GPa in the 4–300 K temperature interval. Resistivity data showed an unusual increase in the thermal energy gap of phase I, which is a semiconductor under ambient conditions. Recently, a similar effect was reported for the 3D topological insulator Bi_2Se_3. Raman spectroscopy studies revealed lattice instability in phase I indicated by the softening of observed vibrational modes with pressure. Our hybrid functional band structure calculations predicted that phase I of Ag_2Se would be a narrow band gap semiconductor, in accordance with experimental results. At a pressure of ~7.5 GPa, Ag_2Se underwent a structural transition to phase II with an orthorhombic *Pnma* structure. The temperature dependence of the resistivity of Ag_2Se phase II demonstrated its metallic character. Ag_2Se phase III, which is stable above 16.5 GPa, is also metallic according to the resistivity data. No indication of the superconducting transition is found above 4 K in the studied pressure range.

Keywords: semiconductor, high pressure, insulator-metal transition

(Some figures may appear in colour only in the online journal)

1. Introduction

High-pressure transport measurement is a powerful tool to investigate pressure-driven changes in the electronic structure of semiconductors. Pressure reduces interatomic distances in materials and may change their properties, most interestingly by reducing the band gap size and causing an insulator-to-metal transition. Materials that show a pressure-induced insulator-to-metal transition are of great interest owing to their potential applications in piezoelectronics.

As a narrow band semiconductor, Ag_2Se has been a material of interest for basic research and technological application for a long time. The low temperature β polymorph [1, 2] that undergoes a transition to the superionic state (α-phase) [3, 4] at elevated temperatures has a band gap smaller than 0.1 eV at 0 K [1]. The β phase of Ag_2Se has an unusually low lattice component of thermal conductivity [5] and a relatively high electrical conductivity and Seebeck coefficient [6]. This makes Ag_2Se a promising candidate for use as a thermoelectric cooling material with an enhanced figure of merit [7].

Both Ag_2Se and Ag_2Te show remarkably large linear magnetoresistance in a wide range of temperatures and magnetic fields [8]. It has been reported that Ag_2Te can act as a topological insulator with an anisotropic Dirac cone [9]. Ag_2Se, however, has not been studied to the same extent. The only high-pressure investigation of electric transport properties was restricted to a determination of the high temperature $\beta - \alpha$ phase transition line [10]. Very recently, the behavior of Ag_2Se was examined at room temperature and pressures up to 20 GPa by means of x-ray diffraction and infrared spectroscopy, combined with evolutionary structure predictions and electronic band structure calculations [11]. Ag_2Se was found to undergo a structural phase transition to phase II (*Pnma* symmetry) at pressures between 7.8 GPa and 10.6 GPa, and to phase III (*Cmcm* symmetry) at a pressure of ~16.5 GPa. The electronic band structure of phase I was shown to have a topologically nontrivial nature; this, combined with the increase in the optical band gap with pressure, was taken as evidence that phase I may be a 3D topological insulator [11]. The observed changes in the infrared spectra with pressure and the calculated electronic band structures demonstrated the metallic nature of high-pressure phases II and III. It is worth confirming the pressure-induced metallization of Ag_2Se by use of direct electric transport measurements. In this paper, we report on the results of electrical resistivity measurements of Ag_2Se at pressures up to 30 GPa, accompanied by x-ray diffraction and Raman spectroscopy characterization of the sample.

2. Experimental and computational details

The Ag_2Se sample was purchased from Sigma Aldrich with a stated purity of 99.99%. For high pressure generation, we used a diamond anvil cell (DAC) with flat culets with a 500 μm diameter.

The structure of the sample in the DAC was characterized at different pressures (all at room temperature) by angle-dispersive x-ray powder diffraction studies performed at the beamline ID09A of the European Synchrotron Radiation Facility (Grenoble, France). No pressure-transmitting medium was used in order to ensure consistency with pressure conditions of subsequent electrical resistivity measurements.

For Raman spectroscopy, the sample was loaded into a 200 μm-thick tungsten gasket pre-indented to a thickness of ~40 μm. Raman spectra were collected in the backscattering geometry on a self-designed Raman optical microscope described elsewhere [12].

For electrical resistivity measurements, the tungsten gasket was insulated with a cubic BN/epoxy mixture. The sample chamber had a diameter of 150 μm and an initial thickness of ~40 μm. The electrical leads were fabricated from 5 μm-thick Pt foil. The pressure dependence of the electrical resistance was measured up to ~30 GPa at temperatures between 4 and 300 K using the DC current van der Pauw technique.

Pressure was measured with an accuracy of ± 0.1 GPa using the ruby luminescence method.

All calculation results presented in this work have been obtained via the Vienna *ab initio* simulation package (VASP) [13], using the projector augmented wave (PAW) [14, 15] method together with a plane-wave cutoff energy of 500 eV. The 4*d* and 5*s* electrons of the Ag pseudopotential and 4*s* and 4*p* electrons of the Se pseudopotential are treated as valence states. In order to provide a good description of the electronic structure, we have used the HSE hybrid functional [16] as the exchange-correlation functional. In the standard implementation of the HSE06 hybrid functional, the values of the range separation parameter ω and the ratio of the exact exchange α are 0.2 $Å^{-1}$ and 0.25, respectively. These parameters were used to perform a structural optimization via total energy, where the atomic structure is considered to be relaxed when the residual forces are below 0.05 eV $Å^{-1}$. The Brillouin-zone integration was performed with a $5 \times 3 \times 3$ mesh of *k*-points centered at the Γ point. The spin–orbit coupling was included in the band structure calculations.

3. Results and discussion

At ambient pressure, Ag_2Se crystallizes into the orthorhombic $P2_12_12_1$ structure ($Z = 4$) [17, 18]. The application of high hydrostatic pressure induces structural phase transitions at 7.8–10.3 GPa and 16.5 GPa to *Pnma* and *Cmcm* structures, respectively [11]. The *ab initio* structural calculations revealed the existence of other low-enthalpy phases, which were observed as minor metastable phases in the experimental diffraction patterns [11]. Thus, the deviatoric stresses due to nonhydrostatic pressure conditions can lead to different structure relations at high pressures. Therefore, we have characterized the structure of the sample in nonhydrostatic conditions (without a pressure-transmitting medium) similar to the pressure conditions for the subsequent electrical resistivity measurements.

Diffraction patterns collected at a pressure of 0.9 GPa, shown in figure 1(a), can be indexed with the ambient pressure orthorhombic $P2_12_12_1$ structure (figure 1(b)) [17, 18] with lattice parameters of $a = 4.334$ Å, $b = 7.079$ Å, and $c = 7.725$ Å. Our Raman spectra of Ag_2Se at low pressures, depicted in figure 2, are in agreement with the published data at ambient pressure [19, 20]. Raman spectra of the $P2_12_12_1$ structure should contain $9A + 8B_1 + 8B_2 + 8B_3$ Raman active modes. Nevertheless, most of them are very weak and located at low frequencies beyond the cut-off of the razor edge filters used in our spectroscopic setup [19]. The spectra observed at the lowest pressure (figure 2) contain two broad weak features at ~155 cm^{-1} and 170 cm^{-1} due to the vibrations of the selenium atoms [19], and a strong peak located at ~230 cm^{-1} due to the symmetric stretching of the Ag–Se tetrahedra (*A*-mode) in agreement with recent Raman spectroscopy data [20].

We note that the strong peak splits into two distinct bands (see figure 2(a)) at pressures above 1.5 GPa. However, this is not an indication of a structural phase transition. The diffraction pattern collected at 3.1 GPa (figure 1(a)) can be unambiguously assigned to the $P2_12_12_1$ structure with lattice parameters of $a = 4.317$ Å, $b = 6.989$ Å, and $c = 7.602$ Å,

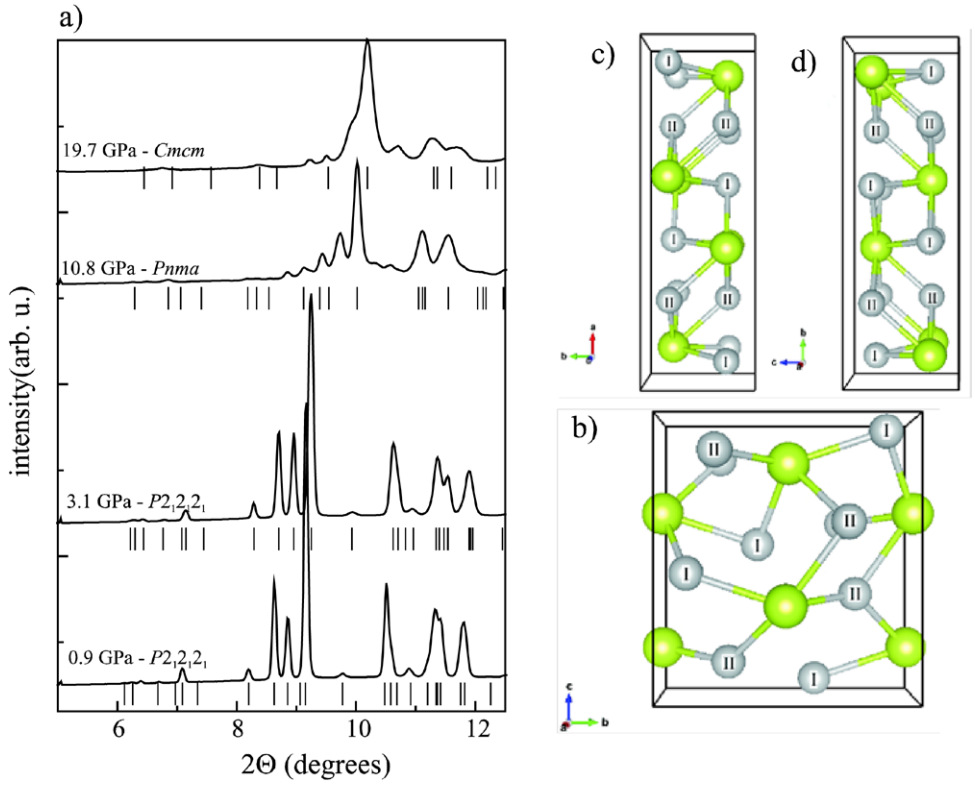

Figure 1. X-ray diffraction patterns of Ag_2Se collected at different pressures (a). Patterns at 0.9 GPa and 3.1 GPa are indexed with phase I $P2_12_12_1$ structure shown on (b). Patterns at 10.8 GPa and 19.7 GPa are indexed with phase II *Pnma* (c) and phase III *Cmcm* (d) structures respectively. The tick marks below each pattern on (a) show the calculated reflection positions of corresponding crystalline structures. The crystallographically inequivalent silver atoms are depicted by gray spheres I and II in (b)–(d), whereas green spheres represent selenium atoms.

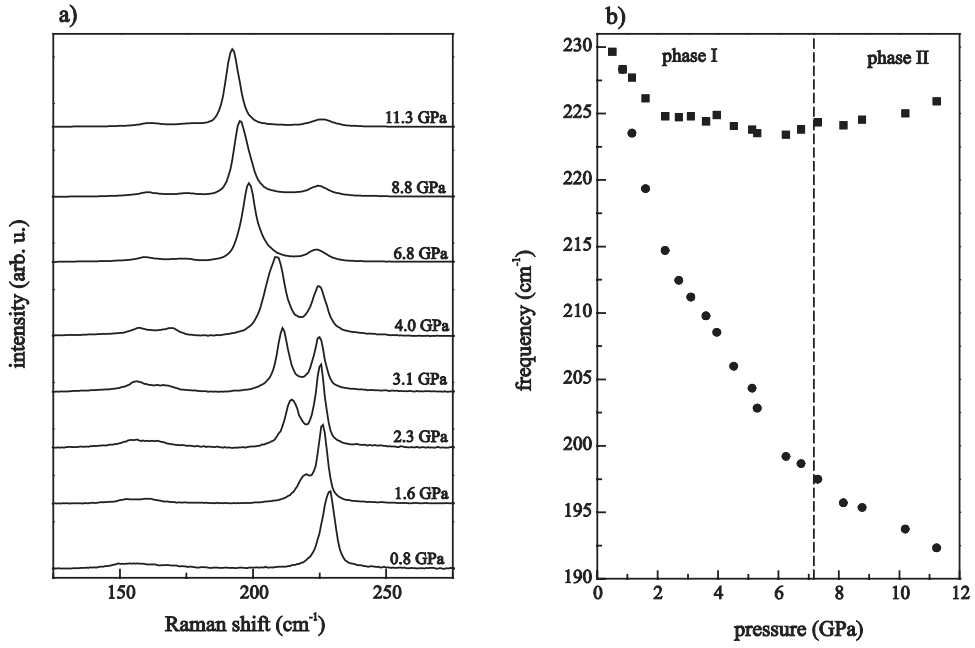

Figure 2. (a) Raman spectra of Ag_2Se at different pressures; (b) pressure dependence of the vibrational modes located at ~230 cm^{-1}.

in good agreement with the recent high pressure studies [11]. The splitting of the vibrational peak illustrates the increasing inequivalence of the two crystallographic sites of Ag atoms (figure 1(b)) due to the highly anisotropic compression of the $P2_12_12_1$ lattice [11]. Another notable feature of the spectra is the continuous decrease in the frequencies of the two Raman peaks under compression (figure 2(b)). This indicates the instability of the $P2_12_12_1$ structure, which triggers the transition to the high-pressure phase II. No considerable changes in the spectra were observed for the phase I–phase II transition,

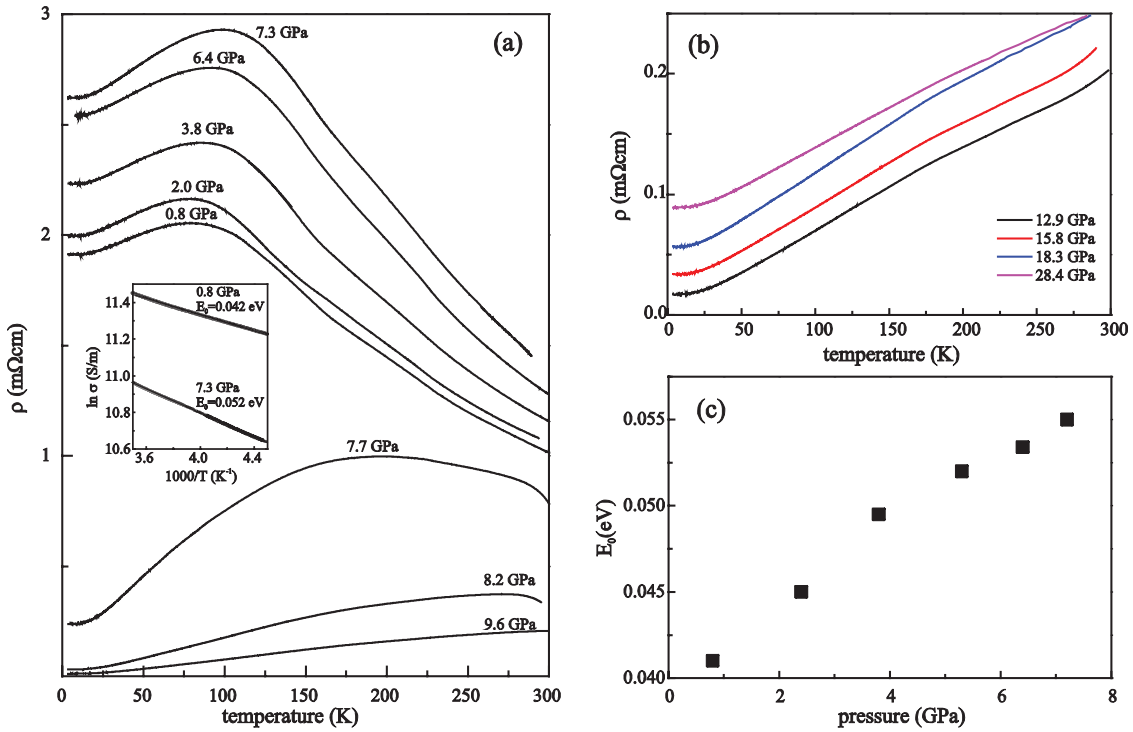

Figure 3. Temperature dependence of the resistivity of Ag_2Se at different pressures (a) and (b). (c) Pressure dependence of the thermal energy gap, obtained from Arrhenius plots shown in the panel (a) inset.

indicating little difference in the coordination of Ag atoms in the course of the transition. Above the pressure at which the phase transition occurs, the higher frequency peak changes to increasing with pressure. At the same time, the lower frequency peak still shows frequency softening with pressure increase. Therefore, the phonon anomaly persists in phase II. Further detailed consideration of Ag_2Se lattice dynamics at high pressure is outside of the scope of this paper and would be a matter of subsequent publication.

The diffraction patterns collected at pressures of 10.8 GPa and 19.7 GPa can be indexed with shown figure 1(c) phase II orthorhombic *Pnma* structure ($a = 12.77$ Å, $b = 4.098$ Å, and $c = 3.932$ Å) and a phase III *Cmcm* (shown on figure 1(d)) structure ($a = 3.835$ Å, $b = 12.494$ Å, and $c = 4.081$ Å), respectively (see figure 1(a)), in agreement with the data obtained for hydrostatic compression [11]. Thus, the nonhydrostatic conditions do not affect the pressure-induced structural phase transitions in Ag_2Se. The high-pressure electrical resistivity data presented below can therefore be attributed to the same phases as in the recently published results [11].

The evolution of the electrical resistivity of Ag_2Se under compression in the temperature range of 3.6–300 K is presented in figures 3(a) and (b). As the pressure increases within the range of stability of phase I, resistivity of Ag_2Se at room temperature increases. A similar trend, i.e. increasing nonmetallicity with pressure, was observed in Bi_2Se_3 topological insulators [21, 22]. This increase in resistivity is connected to the large decrease in carrier mobility due to the changes in the electronic structure induced by high pressure [21].

The resistivity curves recorded at all pressures within the phase I stability range demonstrate non-monotonic dependence of resistivity on temperature, which is typical for narrow-gap semiconductors. At low temperatures (below 80 K), the concentration of charge carriers remains constant and phonon scattering results in increased resistivity with temperature, similar to metallic behavior, while at high temperatures, the intrinsic conductivity becomes activated and resistivity decreases with increasing temperature in accordance with semiconductor behavior. The thermal energy gap of Ag_2Se was calculated from the slope of the Arrhenius plots [1] i.e. $\ln\sigma$ versus $1/T$, as shown in the inset of figure 3(a). The gap increases upon compression, (figure 3(c)) contrary to the usual pressure trend. This observation is in full agreement with the optical band gap increase in Ag_2Se observed in the recent high pressure infrared transmittance studies [11]. A similar pressure induced optical band gap increase was also observed in Bi_2Se_3 3D topological insulators [23]. Based on the results of electronic structure calculations, the authors of [11] considered such band gap behavior in Ag_2Se to be an indication of its potential as a 3D topological insulator.

Table 1. Optimized lattice parameters for different phases at given pressures.

Lattice parameters/ phase (Å)	Phase I (ambient pressure)	Phase II (7 GPa)	Phase III (18 GPa)
a	4.425 (4.405)	13.009	3.857
b	7.157 (7.122)	4.164	12.562
c	7.838 (7.851)	4.041	4.112

Note: The lattice parameters are calculated using the PBE. The values in parentheses are the HSE results for phase I.

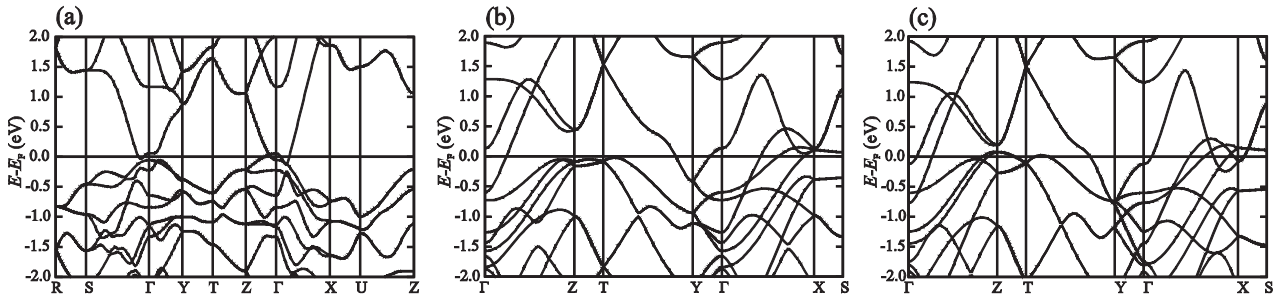

Figure 4. Band structure calculated with the PBE for phase I at ambient pressure (a), phase II at 13 GPa (b), and phase III at 20 GPa (c).

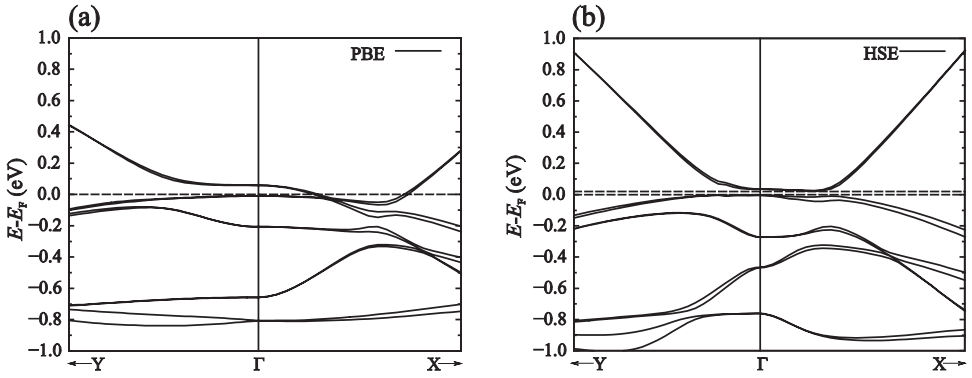

Figure 5. Detailed band structure of phase I around the Γ point near the Fermi level, calculated by PBE (a) and HSE (b).

To confirm our experimental findings, we performed DFT total energy calculations to find the optimized atomic structure of different phases at given pressures. The calculations revealed that up to 7 GPa, phase I is the most stable; at 7 GPa, phase II becomes the most stable and continues to be up to 18 GPa; and at pressures higher than 18 GPa phase III is the most stable. The optimized lattice parameters of the different phases at given pressures are listed in table 1 and are in good agreement with the experimental values.

The optimized electronic band structures for different phases, calculated with PBE at given pressures, are shown in figure 4. The calculated band structure of phase I disagrees with experimental findings, displaying a metallic character at ambient pressure (figures 4(a) and 5(a)). It should be noted that previous results obtained from semilocal approximations to the exchange-correlation functional predict phase I to be a metal as well [11]. This is due to a well-known tendency of semilocal methods to underestimate the band gap of semiconductors. Enabling spin–orbit coupling (SOC) in the band structure calculations prevents band crossing near the Fermi level and may result in a small band gap. The size of the gap predicted by semilocal methods, therefore, is not reliable. Underestimation of the band gap by local and semilocal approximations to the exchange-correlation functional is of particular concern when narrow band gap semiconductors are studied.

A more accurate method is necessary to describe the electronic structure of this class of compounds. We have employed HSE calculations known to predict the band structure of semiconductors accurately. In our band structure calculations, if SOC is not included, the gap is zero for PBE calculations and very small for HSE calculations. Including SOC in the HSE band structure calculations induces a gap near the Fermi energy in agreement with experimental observations (figure 5(b)). In contrast, the band structure obtained from a PBE approximation remains metallic even when SOC is taken into account (figure 5(a)). The value of the band gap calculated by HSE at the Γ point is ~23 meV, which is in reasonable agreement with the experimental data. The calculated band structures of phase II at 13 GPa (figure 4(b)) and phase III at 20 GPa (figure 4(c)) are similar to the previously reported theoretical results [11] and illustrate the metallic character of both high-pressure phases, in agreement with experimental observations described below.

As pressure is increased above 7.3 GPa, to the range where phase II is more stable, the resistivity of the sample significantly decreases (figure 3(a)). At pressures above 8 GPa, the resistivity curves show metallic behavior throughout the whole temperature range of 4–300 K (figure 3(b)). Thus, our electrical resistivity measurements confirm the metallic nature of phase II suggested by infrared reflectivity measurements and electronic structure calculations [11]. It is worth noting that at the transition to phase II the shortest distance between Ag atoms decreases to 2.84–3.0 Å, becoming comparable to the interatomic distances in pure Ag (2.89 Å). This atomic distribution of silver atoms may explain the metallic conductivity of Ag_2Se at high pressure.

The sample remained metallic at further pressure increases up to 30 GPa. No considerable changes in the resistivity were observed when the phase II–phase III transition (at a pressure

of ~16.5 GPa) occurred (figure 3(b)). The minor structural changes occurring in the course of this transition evidently do not affect the electric transport properties. This is also in agreement with the results of the theoretical calculations, which give similar electronic band structures for phase II (figure 4(b)) and phase III (figure 4(c)). The main difference between the phase II and phase III structures is the broadening of the bands in phase III, resulting in enhancement of the metallic states. We did not find any evidence of superconductivity in the sample at pressures up to 30 GPa and temperatures down to 4 K.

4. Conclusions

The pressure dependence of the electrical resistivity in the narrow band gap semiconductor Ag_2Se was studied at pressures up to ~30 GPa. Our experiments and band structure calculations indicate that phase I (which is stable below 7 GPa) is a narrow gap semiconductor. The results of electronic band calculations performed with the HSE hybrid functional are in agreement with experimental observations for this semiconductor state. The thermal energy gap of phase I increases upon compression, which is unusual. The increase in the room-temperature resistivity with pressure indicates increasing phase I nonmetallicity. Our findings correlate very well with the data from recent infrared absorption studies. A similar effect was observed recently in the 3D topological insulator Bi_2Se_3. Our Raman spectroscopy studies revealed the softening of the observed vibrational modes, indicating the structural instability of low-pressure phase I with a $P2_12_12_1$ structure. Using direct electrical resistivity measurements, we demonstrated that at a pressure of ~7.5 GPa, Ag_2Se undergoes a semiconductor-to-metal transition. Electronic band structure calculations confirm the metallic character of the high-pressure phases of Ag_2Se. Superconductivity was not observed in the sample within the pressure–temperature range studied.

Acknowledgments

We acknowledge the European Synchrotron Radiation Facility for granting the beamtime and we would like to thank Dr M Hanfland for the assistance in using the beamline ID-09.

References

[1] Dalven R and Gill R 1967 *Phys. Rev.* **159** 645
[2] Dalven R and Gill R 1967 *J. Appl. Phys.* **38** 753
[3] Junod P 1959 *Helv. Phys. Acta* **32** 567
[4] Shukla A K, Vasan H N and Rao C N R 1981 *Proc. R. Soc.* A **376** 619
[5] Taylor P F and Wood C 1961 *Adv. Energy Convers.* **1** 141
[6] Simon R, Bourke R E and Lougher E H 1963 *Adv. Energy Convers.* **3** 481
[7] Ferhat M and Nagao J 2000 *J. Appl. Phys.* **88** 813
[8] Xu R, Husmann A, Rosenbaum T F, Saboungi M L, Enderby J E and Littlewood P B 1997 *Nature* **390** 57
[9] Zhang W, Yu R, Feng W, Yao Y, Weng H, Dai X and Fang Z 2011 *Phys. Rev. Lett.* **106** 156808
[10] Banus M D 1965 *Science* **147** 732
[11] Zhao Z, Wang S, Oganov A R, Chen P, Liu Z and Mao W L 2014 *Phys. Rev.* B **89** 180102
[12] Medvedev S A, Barkalov O I, Naumov P, Palasyuk T, Evers J, Klapötke T M and Felser C 2015 *J. Appl. Phys.* **117** 165901
[13] Kresse G and Furthmüller J 1996 *Phys. Rev.* B **54** 11169
[14] Blöchl P E 1994 *Phys. Rev.* B **50** 17953
[15] Kresse G and Joubert D 1999 *Phys. Rev.* B **59** 1758
[16] Heyd J, Scuseria G E and Ernzerhof M 2003 *J. Chem. Phys.* **118** 8207
[17] Billetter H and Ruschewitz U 2008 *Z. Anorg. Allg. Chem.* **634** 241
[18] Yu J and Yun H 2011 *Acta Cryst.* E **67** i45
[19] Ishii M and Wada H 1993 *Mater. Res. Bull.* **28** 1269
[20] Pandiaraman M and Soundararajan N 2012 *J. Theor. Appl. Phys.* **6** 7
[21] Hamlin J J, Jeffries J R, Butch N P, Syers P, Zocco D A, Weir S T, Vohra Y K, Paglione J and Maple M B 2012 *J. Phys.: Condens. Matter* **24** 035602
[22] Zhang J, Han Y, Liu C, Zhang X, Ke F, Peng G, Ma Y, Ma Y and Gao C 2014 *Appl. Phys. Lett.* **105** 062102
[23] Segura A *et al* 2012 *Phys. Rev.* B **85** 195139